Atmospheric Environment 147 (2016) 67–78

Contents lists available at ScienceDirect

Atmospheric Environment

journal homepage: www.elsevier.com/locate/atmosenv

Quantifying organic aerosol single scattering albedo over the tropical biomass burning regions☆

Jung-Eun Chu [a, b], Kyung-Ja Ha [a, b, c, *]

[a] Division of Earth Environmental System, College of Natural Science, Pusan National University, Busan, Republic of Korea
[b] Research Center for Climate Sciences, Pusan National University, Busan, Republic of Korea
[c] Department of Atmospheric Sciences, Pusan National University, Busan, Republic of Korea

HIGHLIGHTS

- A creative method for determining OA SSA is suggested.
- Observation-based retrieval reveals OA SSA of 0.91.
- Observationally constrained global mean sulfate and nitrate AOD is 0.017.
- The global aerosol direct radiative forcing can be lower than currently believed.

ARTICLE INFO

Article history:
Received 28 March 2016
Received in revised form
26 September 2016
Accepted 29 September 2016
Available online 29 September 2016

Keywords:
Aerosol light absorption
Brown carbon
Organic aerosol
Sulfate
Nitrate

ABSTRACT

Despite growing evidence of light-absorbing organic aerosols (OAs), their contribution to the Earth's radiative budget is still poorly understood. In this study we derived a new empirical relationship that binds OA single scattering albedo (SSA), which is the ratio of light scattering to extinction, with sulfate + nitrate aerosol optical depth (AOD) and applied this method to estimate OA SSA over the tropical biomass burning regions. This method includes division of the attribution of black carbon (BC) and OA absorption aerosol optical depths from the Aerosol Robotic Network (AERONET) observation and determination of the fine-mode ratio of sea-salt and dust AODs from several atmospheric chemistry models. Our best estimate of OA SSA over the tropical biomass burning regions is 0.91 at 550 nm. Uncertainties associated with observations and models permit a value range of 0.82–0.93. Furthermore, by using the estimated OA SSA and comprehensive observations including AERONET, Moderate Resolution Imaging Spectroradiometer (MODIS) and Multi-angle Imaging Spectroradiometer (MISR), we examined the first global estimate of sulfate + nitrate AOD through a semi-observational approach. The global mean sulfate + nitrate AOD of 0.017 is in the lower range of the values obtained from 21 models participated in AeroCom phase II. The results imply that most aerosol models as well as climate models, which commonly use OA SSA of 0.96–1.0, have so far ignored light absorption by OAs and have overestimated light scattering by sulfate + nitrate aerosols. This indicates that the actual aerosol direct radiative forcing should be less negative than currently believed.

1. Introduction

During the last decade, light absorption by atmospheric aerosols has attracted significant attention because of its huge impact on regional climate and the Earth's radiation balance. In the solar spectrum, under cloud-free conditions, direct radiative forcing by atmospheric aerosols is usually negative at the top of the atmosphere (TOA); however, it can become less negative or even positive with increasing aerosol absorption (Boucher et al., 2013; Feng et al., 2013). Studies regarding aerosol light absorption have considered black carbon (BC) as a single light absorbing species. During the last 10 years, laboratory and field experiments have provided strong evidence of the fact that some organic aerosols (OAs) absorb a substantial amount of sunlight, whereas others only scatter sunlight (Kirchstetter et al., 2004; Andreae and Gelencsér, 2006;

☆ Submitted to Atmospheric Environment.

* Corresponding author. Department of Atmospheric Sciences, Pusan National University, Busan 609-735, Republic of Korea.
E-mail address: kjha@pusan.ac.kr (K.-J. Ha).

http://dx.doi.org/10.1016/j.atmosenv.2016.09.069
1352-2310/

Alexander et al., 2008; Chen and Bond, 2010; Chung et al., 2012; Lack et al., 2012). The evidence for the presence of light absorbing OAs originates from the spectral dependence of light absorption that cannot be explained by BC absorption near specific combustion sources. OAs that absorb sunlight appear brownish owing to their strong solar absorption toward shorter visible and ultraviolet radiation; therefore, such OAs are known as brown carbon (BrC; Andreae and Gelencsér, 2006). The origins of atmospheric OAs are the incomplete combustion of biomass (Reid et al., 2005; Hoffer et al., 2006; Chakrabarty et al., 2010; Lack et al., 2013; Forrister et al., 2015) and fossil fuels (Bond, 2001; Yang et al., 2009; Zhang et al., 2011) and the secondary formation from gas-phase organic compounds (Laskin et al., 2014; Nakayama et al., 2013; Yu et al., 2014). The OAs make up more than 80% of fine-particle mass in the atmosphere in tropical savannas (Magi, 2009) where tens to hundreds of mega hectares are burned every year (Giglio et al., 2013) (Fig. 1). However, there are various OA source materials and chemical composition; therefore, it is difficult to generalize optical properties of OAs (Kanakidou et al., 2005).

The aerosol light absorption can be quantitatively expressed by using single scattering albedo (SSA) which is defined by the ratio of aerosol light scattering to aerosol light extinction (the sum of absorption and scattering). For non-absorbing aerosols the SSA is 1. It is crucial to exactly understand the SSA of aerosol since the sensitivity in aerosol direct radiative forcing is primarily driven by differences in SSA (Abel et al., 2005; Magi et al., 2008) rather than the absolute value of absorption, and hence even small error in its estimation can change the sign of aerosol radiative forcing (Yamamoto and Tanaka, 1972; Takemura et al., 2002; Kanakidou et al., 2005). Large uncertainties exist, however, in the measurement of OA light absorption from both laboratory experiments and field observations, which tend to cause substantial overestimation of OA light absorption. For example, the extraction of laboratory generated aerosol samples with organic solvents prior to thermochemical analysis generally shows greater absorption than those not extracted (Chen and Bond, 2010). In addition, the most commonly used in situ instruments for measuring aerosol light absorption, including the Aethalometer (Magee Scientific Co., Berkely, CA) and the Particle Soot Absorption Photometer (Radiance Research, Seattle, WA), tend to overestimate aerosol light absorption because the absorption is enhanced by backscattering and multiple scattering (Chow et al., 2009).

Providing long-term, continuous, and readily available aerosol observation, the ground-based worldwide network of automatic sun- and sky-scanning measurements, Aeronet Robotic Network (AERONET; Holben et al., 1998, 2001), has been used throughout the literature to determine aerosol optical properties near specific source regions (Russell et al., 2010; Giles et al., 2012). However, these observations yield column-integrated measurements and therefore include different aerosols and mixing states. To make the best use of AERONET data, there is a need for additional work in characterizing light absorption by individual aerosol species. However, due to the difficulties in separating contribution of individual species to total light absorption, only few studies tried to partition OA light absorption using AERONET (Bahadur et al., 2012; Chung et al., 2012).

The main purpose of this study is the development of an algorithm to derive OA SSA empirically and the determination of OA SSA over the tropical biomass burning regions. In particular, we develop an algorithm that binds OA SSA with sulfate + nitrate AOD mostly by using ground-based AERONET data. The algorithm partly employs the ensemble mean of model simulations. We apply this empirical algorithm to determine the OA SSA over the tropical biomass burning regions by using the sulfate + nitrate AOD measured during the Southern African Research Initiative field campaign in August and September 2000 (SAFARI-2000) (Swap et al., 2003). The uncertainties from observations and the retrieval algorithm are extensively considered in estimating the range of OA SSA. Our method is different from that of Bahadur et al. (2012) in that there is no assumption of OA light absorption at higher wavelengths, and the OA SSA is determined from the amount of measured sulfate + nitrate AOD. It should be also pointed out that there are large differences in individual aerosol composition among models, and the model diversity of each of aerosol component will introduce large uncertainties to the aerosol-associated solar direct radiative forcing (Kinne et al., 2006). The biases provide an additional motivation for examining observation-based retrieval of individual aerosol species such as light scattering sulfate and nitrate aerosols. We further provide the first global estimate of sulfate + nitrate AOD constrained mostly by observations using the empirically derived OA SSA.

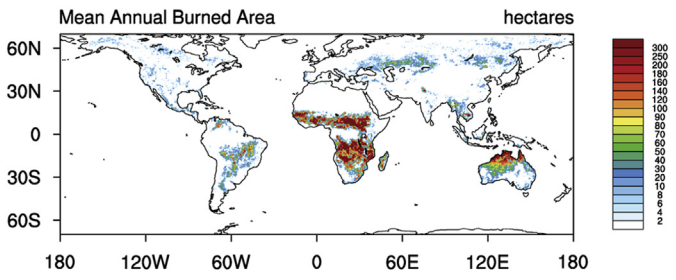

Fig. 1. Mean annual burned area in units of hectares at 0.25° spatial resolution derived from the January 1996 to December 2013 data of the monthly Global Fire Emissions Database fourth version (GFED4; Giglio et al., 2013). The annual mean was computed by the unweighted sum of 12-month data that were then averaged over 18 years.

2. Data and methods

2.1. Data

In this section, we describe the data obtained from the observations and global aerosol simulations. All data are monthly means and are interpolated to the T42 resolution, approximately 2.8° × 2.8°. Unless otherwise noted, we use optical variables at a wavelength of 550 nm. Table 1 shows a summary of the symbols and acronyms used in this paper.

2.1.1. AERONET

AERONET is a ground-based remote sensing maintained by the National Aeronautics and Space Administration (NASA) Goddard Space Flight Center (Holben et al., 1998, 2001). Although this automatic sun- and sky-scanning measurement does not cover the whole globe, its wide angular and spectral measurement provides most reliable and continuous aerosol optical properties in key locations (Dubovik et al., 2002). The AERONET AOD is known to be the most accurate global-scale product, and the uncertainty range

Table 1
Summary of acronyms and symbols used in this study.

Symbol	Acronym	Description
τ	AOD	Aerosol optical depth (from surface to TOA)
τ_a	AAOD	Absorption aerosol optical depth (=(1 − SSA) × AOD)
τ_f	fAOD	Fine-mode aerosol optical depth
τ_c	cAOD	Coarse-mode aerosol optical depth
α	AE	Ångström exponent for AOD
β	AAE	Absorption Ångström exponent
ω	SSA	Single scattering albedo

of its derived AOD is 0.01–0.02 owing mainly to calibration (Holben et al., 1998, 2001; Eck et al., 1999); its calibrated sky radiance measurements typically have uncertainty of less than 5% (Holben et al., 1998, 2001). We downloaded the AERONET Version 2 product AOD at four wavelengths of 440, 675, 870, and 1020 nm from the direct sun measurement from 2001 to 2010. Cloud-screened and quality-assured Level 2 almucantar retrieval sensitivity requires high aerosol loading (>0.3 at 440 nm) and large solar zenith angles (>50°) with an accuracy of ~0.03 which may yield sampling bias (Dubovik et al., 2002). Fine-mode AOD (fAOD) at 500 nm is obtained from the spectral deconvolution algorithm (SDA) (O'Neill et al., 2001a,b; O'Neill, 2003)). We used the monthly mean AOD and fAOD for the monthly FMF rather than averaging daily FMFs. The coarse-mode AOD (cAOD) was obtained by subtracting fAOD from AOD. We obtained fAOD at 550 nm by subtracting the cAOD at 500 nm from the total AOD at 550 nm, assuming that the cAOD does not change from 500 to 550 nm. The AAOD was obtained from the monthly AOD multiplied by 1-SSA. The AERONET AE and AAE were computed by the linear regression of the log–log space using AOD and AAOD at 440, 675, and 870 nm. The climatology was computed by taking the 2001–2010 average for each calendar month.

2.1.2. Fine-mode sea-salt and dust AODs

We used the multi-model mean for fine-mode dust (fdust) and fine-mode sea-salt (fss) AODs. Because dust and sea-salt aerosols are predominantly large particles, not all aerosol and climate models simulate small dust and sea-salt AODs. We collected three models that simulate fdust and fss AODs: Goddard Chemistry Aerosol Radiation and Transport (GOCART), Tracer Model 5 (TM5), and ModelE2-Two-Moment Aerosol Sectional (TOMAS). For the GOCART simulations, we used the sea-salt AOD from Chin et al. (2002) and the dust AOD from the Giovanni website (http://gdata1.sci.gsfc.nasa.gov/daac-bin/G3/gui.cgi?instance_id=neespi), which contains the GOCART model output from 2000 to 2007. The TM5 output was obtained from a simulation prepared for the Aerosol Comparison between Observations and Models (AeroCom) phase III hindcast experiment (Huijnen et al., 2010). The ModelE2-TOMAS microphysics model (Adams and Seinfeld, 2002) is incorporated into the state-of-the-art general circulation model (GCM) Goddard Institute for Space Studies (GISS) ModelE2 (Lee et al., 2015). The TOMAS module represents the aerosol size distribution in many size categories or bins from 10 nm to 10 μm. We used the Fast-TOMAS module with a 15-bin version because, compared with the original TOMAS model with 30 bins, it reduces the computational burden by two–three times while effectively preserving the capability of computing the FMF. The fAOD for both dust and sea-salts were calculated by multiplying the AOD by the FMF. The FMF of dust and sea-salt aerosols from ModelE2-TOMAS was calculated by converting the mass output to AODs and then applying the SDA algorithm used in AERONET retrieval (O'Neill et al., 2001a,b; O'Neill, 2003) to the AODs in order to create FMF consistent with AERONET FMF. For computing the size-resolved AODs at 380, 440, 500, 675, and 870 nm, a Mie-scattering code was applied using the refractive index taken from the Optical Properties of Aerosol and Clouds (OPAC) dataset (Hess et al., 1998). The climatological AODs for all three models were obtained by averaging the simulation periods of 2000–2007, 2001–2010, and 2003–2005 for GOCART, TM5, and ModelE2-TOMAS, respectively. The annual mean climatological AODs were obtained by taking the average of the climatology for each calendar month.

2.1.3. Sulfate + nitrate AOD

We prepared the sulfate + nitrate AODs from 21 models participated in AeroCom phase II project (Schulz et al., 2006; Schulz et al., 2009) for comparison with the sulfate + nitrate AOD estimated in this study. The AeroCom-project is an open international initiative of scientists that aims for further understanding of global aerosols and their impact on climate. We adopted 19 models from the AeroCom control run (CTRL_2006) that was proposed as a reference and control simulation based on the emissions for 2006. In addition, two models, Spectral Radiation-Transport Model for Aerosol Species (SPRINTARS) and TM5, were adopted from the AeroCom hindcast run of the Intergovernmental Panel on Climate Change (HCA-IPCC) in which meteorology and sea surface temperature (SST) have yearly variability. For comparison with the 2001–2010 observations, SPRINTARS data were averaged for the period 2000–2008, whereas TM5 data were averaged for 2000–2009. The details of the diagnostics required are available on the AeroCom website (http://aerocom.met.no/). Table 2 lists the model names, data availability for sulfate and nitrate AODs, and original resolutions of each model. Among 21 models, 5 models simulated nitrate AOD. We modified these models with missing aerosol information (i.e., nitrate AOD) by accounting for the multi-model mean nitrate AOD. We evaluated the performance in five models in simulating nitrate AOD over the most abundant source region, central Eastern China (30°N-41.5°N, 110°E-122°E), in comparison with in a previous study that obtained nitrate AOD from a combination of satellite-retrieved AOD and a chemistry transport model (CTM) using a data assimilation technique (Park et al., 2014). Since two models differ by a factor of 10 from Park et al. (2014), we selected three models and calculated the mean of nitrate AOD from the three models. Then we added the three model averaged nitrate AOD to the models that does not treat it. The three models are global monsoon Global Modeling Initiative (GMI), GMI-v3, and Hadley Centre Global Environmental Model version 2 (HadGEM2-ES). Because the global mean AOD can be affected by the model resolution, the original data were re-gridded by interpolation to the common T42 grid prior to any statistical analysis.

2.2. Methods

In this section, we introduce the method used to derive OA SSA empirically from the combination of AERONET and model outputs. We used mostly ground-based AERONET observations; a minor part included multi-model mean simulations. Fig. 2 shows a simplified process flow chart for deriving OA SSA.

Beginning from AERONET fAOD, the fAOD consists mostly of sulfate + nitrate, BC, and OA aerosols mostly derived from anthropogenic sources, whereas a sizable portion of dust and sea-salt aerosols consist of fine-mode particles. Because optical depth is an additive quantity, the scattering and absorption of each aerosol species can be treated separately, as shown in Eq. (1).

$$\tau_f(\lambda) = \tau_{\text{sulfate+nitrate}}(\lambda) + \tau_{BC}(\lambda) + \tau_{OA}(\lambda) + \tau_{\text{fdust}}(\lambda) + \tau_{\text{fss}}(\lambda) \quad (1)$$

As will be subsequently discussed, we derived the contributions of BC and OA AODs by separating BC and OA AAODs from AERONET total AAOD. The fdust and fss values were derived from the multi-model mean (see Section 2.1.2). Therefore, in Eq. (1), sulfate + nitrate AOD is a unique term that is not obtained from observation or model simulation. It should be also noted that sulfate and nitrate aerosols are often treated together as a sulfate–nitrate–ammonia system because both sulfate and nitrate aerosols are formed in the atmosphere through oxidation and neutralization of precursor gases such as sulfur dioxide and nitrogen, and the most abundant acids in the troposphere are sulfuric acid and nitric acid; ammonia acts as the main neutralizing agent for these species (Wang et al., 2013). Hereafter, we refer to

Table 2
Model names, data availability for sulfate and nitrate, and original resolutions used in AeroCom phase II models.

Experiment name	Model name (period)	Sulfate (SO4)	Nitrate (NO3)	Resolution (nx × ny)
HCA-IPCC	SPRINTARS (2000–2008)	O	X	320 × 160
	TM5 (2000–2009)	O	O	120 × 90
CTL_2006	BCC_AGCM2.0.1_CAM	O	X	128 × 64
	CAM5.1-MAM3-PNNL	O	X	144 × 96
	CAM5-MAM3-PNNL	O	X	144 × 96
	ECHAM-SALSA	O	X	192 × 96
	GEOS_CHEM_APM_ant	O	X	72 × 46
	GEOS_CHEM_APM_nat	O	X	72 × 46
	GMI	O	O	144 × 91
	GMI-v3	O	O	144 × 91
	GOCART-v4Ed	O	X	144 × 91
	HadGEM2-ES	O	O	192 × 145
	HadGEM2-ESv0	O	X	192 × 145
	MPIHAM_V1_KZ	O	X	192 × 96
	MPIHAM_V2_KZ	O	X	192 × 96
	OsloCTM2	O	X	128 × 64
	SALSA_V1_TB	O	X	128 × 64
	SPRINTARS-v384	O	X	320 × 160
	SPRINTARS-v385	O	X	320 × 160
	TM4-ECPL-F	O	X	120 × 90
	TM5-V3	O	O	120 × 90

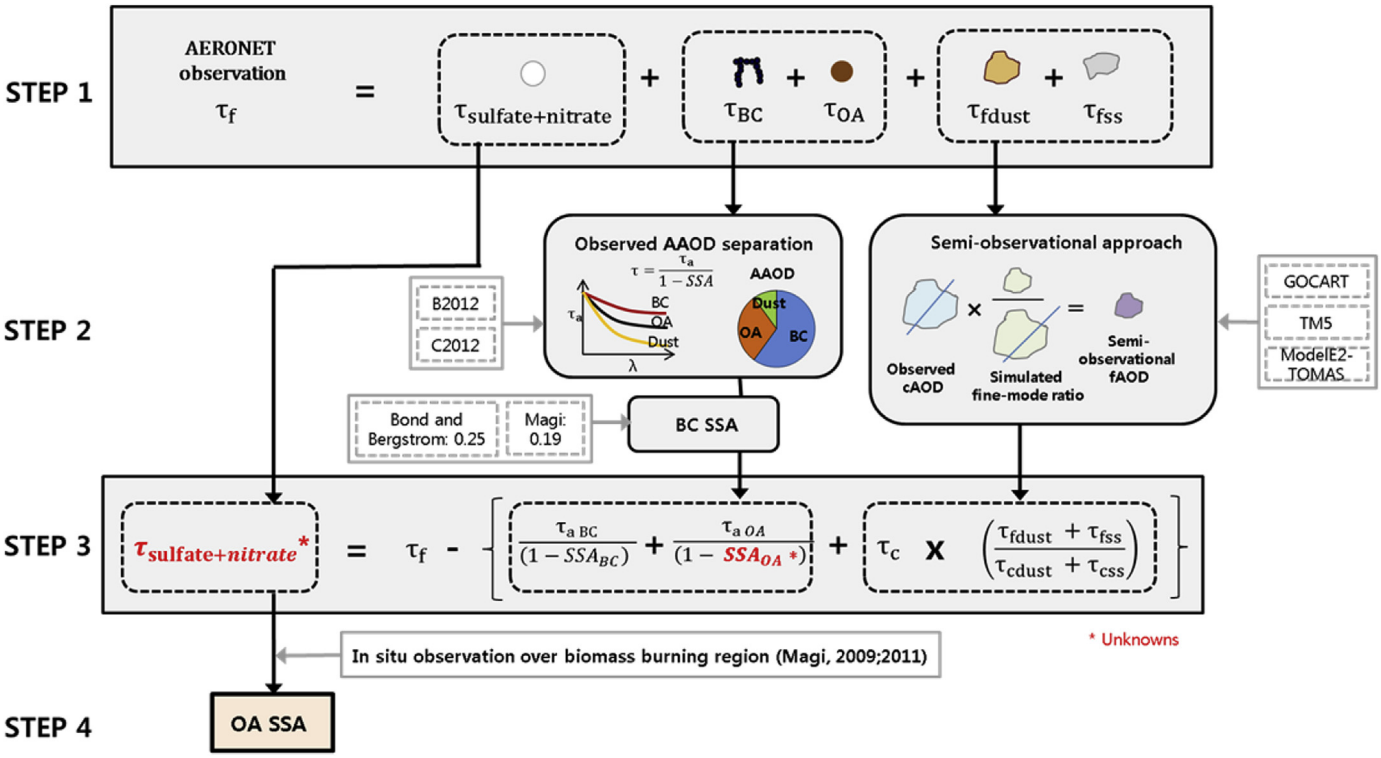

Fig. 2. Flow chart showing the procedure used for deriving OA SSA.

sulfate + nitrate aerosols as the sum of sulfate and nitrate aerosols. Moving the sulfate + nitrate AOD term to the left–hand side and replacing AOD with AAOD divided by 1-SSA, Eq. (1) is rewritten as Eq. (2).

$$\tau_{\text{sulfate+nitrate}}(\lambda) = \tau_{\text{f}}(\lambda) - \left(\frac{\tau_{a_{\text{BC}}}(\lambda)}{1-\text{SSA}_{\text{BC}}} + \frac{\tau_{a_{\text{OA}}}(\lambda)}{1-\text{SSA}_{\text{OA}}} + \tau_{\text{fdust}}(\lambda) + \tau_{\text{fss}}(\lambda)\right) \quad (2)$$

The next step was to derive the contributions of BC and OA AAODs to the total AAOD. To the best of our knowledge, two previous studies by Chung et al. (2012) and Bahadur et al. (2012) suggested BC and OA partitioning method by using the observed AAOD and its wavelength dependence. For convenience, we refer to these studies as C2012 and B2012 respectively. The partitioning method basically assumes that the wavelength dependence of AOD and AAOD, i.e., Ångström Exponent (AE) and Absorption Ångström Exponent (AAE), are intrinsic properties of individual aerosols and are not dependent on the mixing state. The wavelength

dependence of the AAOD captures the aerosol intrinsic properties and is expressed by the following equation, where $(\lambda^R) = 550$ nm is the reference wavelength:

$$\tau_a(\lambda) = \tau_a(\lambda_R)\cdot[\lambda/\lambda_R]^{-\beta} \quad (3)$$

With respect to AAOD, BC, OA and dust aerosols are primary contributors. Dust aerosols have different emission sources from those of combustion-related carbonaceous aerosols (CA) which consists of BC and OA, and distinct wavelength dependences of absorption and scattering. For example, dust AAOD increases steeply toward shorter wavelengths, whereas that of CA is much less steep (Russell et al., 2010; Chung et al., 2012). C2012 distinguished the dust absorption first from CA and solved CA AAOD and dust AAOD by using two wavelengths, 550 and 675 nm, from the given CA AAE and dust AAE. B2012 selected dust-free, dust-dominated, and BC-dominated AERONET sites and applied AAEs at two wavelength ranges, 440–675 nm and 675–870 nm, with the assumption that AAE at 870 nm is entirely due to BC. The AAE values used in C2012 and B2012 are summarized in Table 3. Both C2012 and B2012 used AAE values from sites typically dominated by specific sources related to dust, BC, and OA.

Although fdust and fss aerosols are predominantly natural aerosols, these species have not been observed globally. Therefore, we used a semi-observational approach by combining the simulated fine-mode ratio of dust and sea-salt AODs with the cAOD derived from AERONET (Section 2.1.1 and 2.1.2). We used model simulations from GOCART, TM5, and ModelE2-TOMAS. Details on the model description are explained in Section 2.1.2. Although fdust and fss make a small contribution to the particulate mass in tropical biomass burning regions, the model-to-model difference in fdust + fss AOD is comparable to or even larger than the single model value, which creates difficulty in evaluating the overall model skill. Therefore, caution should be taken in applying our algorithm to other regions such as dust and sea-salt source regions. To minimize the uncertainties arising from model simulations, we adopted the fine-mode ratio of dust + sea-salt AOD, (fdust + fss)/(cdust + css), and multiplied the resultant value with the observed cAOD rather than using the fine-mode AODs directly. An underlying assumption is that cAOD results only from sea-salt and dust aerosols. The last two terms on the right in Eq. (2) become

$$\tau_{fdust}(\lambda) + \tau_{fss}(\lambda) = \tau_c(\lambda) \times \left(\frac{\tau_{fdust}(\lambda) + \tau_{fss}(\lambda)}{\tau_{cdust}(\lambda) + \tau_{css}(\lambda)}\right) \quad (4)$$

When Eq. (2) and Eq. (4) are combined, the final sulfate + nitrate AOD at the wavelength λ is determined as

$$\tau_{sulfate+nitrate}(\lambda) = \tau_f(\lambda) - \left[\frac{\tau_{a_{BC}}(\lambda)}{1-SSA_{BC}} + \frac{\tau_{a_{OA}}(\lambda)}{1-SSA_{OA}} + \tau_c(\lambda) \times \left(\frac{\tau_{fdust}(\lambda) + \tau_{fss}(\lambda)}{\tau_{cdust}(\lambda) + \tau_{css}(\lambda)}\right)\right] \quad (5)$$

where fAOD and cAOD are obtained directly from observations, BC and OA AAODs are partitioned from the observed AAOD, and the fine-mode ratio of dust + sea-salt AOD is obtained from the multi-model mean.

With regard to BC SSA, Bond and Bergstrom (2006) summarized the measured values of freshly generated BC SSA and recommended values of 0.20–0.30 fresh BC aerosol with a central value of about 0.25. In the ambient atmosphere, BC SSA increases when BC is mixed with other components (Cross et al., 2010). Accounting for BC coated by scattering aerosols, Magi (2009, 2011) analyzed field data over regions dominated by biomass burning and obtained a value of 0.14–0.24 with a central value of 0.19. We used the measured BC SSAs both from Magi (2009, 2011) and Bond and Bergstrom (2006). Adopting BC SSA from the measured value, Eq. (5) predominantly becomes an observationally constrained approach for determining the sulfate + nitrate AOD in which the equation has a sole parameter (i.e., OA SSA).

Because general field observations measure the amount of sulfate + nitrate AOD relative to the fAOD, Eq. (5) divided by fAOD yields:

$$\frac{\tau_{sulfate+nitrate}(\lambda)}{\tau_f(\lambda)} = 1 - \frac{\frac{\tau_{a_{BC}}(\lambda)}{1-SSA_{BC}} + \frac{\tau_{a_{OA}}(\lambda)}{1-SSA_{OA}} + \tau_c(\lambda) \times \left(\frac{\tau_{fdust}(\lambda)+\tau_{fss}(\lambda)}{\tau_{cdust}(\lambda)+\tau_{css}(\lambda)}\right)}{\tau_f(\lambda)} \quad (6)$$

which is an applied version of Eq. (5).

At a minimum, our methodology has the following uncertainties: (1) separation of BC AAOD and OA AAOD, (2) the use of model simulations for fdust and fss, and (3) the use of measured BC SSA. Quantitative comparisons will be made in section 3 by considering all uncertainty factors.

Table 3
Absorption Ångström Exponent (AAE) values and dust-free conditions used for AAOD separation methods in C2012 and B2012 over biomass burning regions.

Species	Chung et al. (2012)	Bahadur et al. (2012)	
	$AAE_{440\text{-}675\text{-}870}$	$AAE_{440\text{-}675}$	$AAE_{675\text{-}870}$
CA	1.14 ± 0.24	1.17 ± 0.40	1.23 ± 0.40
Dust	2.42 ± 0.20	2.20 ± 0.50	1.15 ± 0.50
BC	0.50 ± 0.12	0.55 ± 0.24	0.83 ± 0.40
OA	4.80 ± 1.25	4.55 ± 2.01	–
Dust-free	AAE>1.14	$AE_{440\text{-}675}$>1.2, $AAE_{675\text{-}870}/AAE_{440\text{-}675}$ > 0.8	

3. Result

3.1. Sensitivity tests

3.1.1. Sensitivity for AAOD separation methods

Before applying the empirical relationship between OA SSA and sulfate + nitrate AOD, we performed sensitivity tests in order to examine differences in AAOD separation methods and fine-mode sea-salt and dust AODs. In this section, we examined the differences in BC and OA AAOD separation methods between C2012 and B2012. First, we selected the AERONET sites representative of biomass-burning-dominated regions. The atmospheric particulate matters from biomass burning typically consist of fine particles with a large fraction of BC and OA. Therefore, the observed columnar aerosol optical properties over biomass-burning-dominated region exhibit relatively smaller SSA and larger FMF and AE than other source regions (Giles et al., 2012). We defined biomass-burning-dominated sites as having monthly observed data with SSA <0.85, FMF >0.80, and AE > 1.0 at 550 nm over non-industrial areas (Giles et al., 2012). The condition of non-industrial areas was included to avoid confusion with industrial BC mixed with other inorganic particles; these areas were roughly distinguished from those with fossil fuel combustion in southern Asia, Eastern Europe, and North America. Fig. 3(a) shows that the 41

chosen sites and the locations agree well with the annual mean burned area given in Fig. 1. More than one-third of the chosen sites are located in southern Africa; the others are located in central South America, southern North America, Southeast Asia, and northern Australia. Large biomass burning areas in central Africa were not included because of the internal and external mixing of biomass burning particles with dust aerosols transported from the Sahara desert and the consequential reduction in FMF.

Fig. 3(b) shows BC AAOD and OA AAOD retrieved from the method in C2012 and B2012 over the 41 biomass-burning-dominated sites. The distinguished BC AAODs from both separation methods show very similar values for all chosen biomass burning sites. The correlation coefficient between BC AAODs from B2012 and that of C2012 is 0.99. On average, BC AAOD values retrieved from the method of B2012 were 9% higher than those of C2012 owing mainly to differences in the definition of dust-free conditions. The OA AAOD values from the method of B2012 were on average 14% higher than that of C2012; however, 17 of 41 sites had lower OA AAOD values than those retrieved by C2012. The correlation coefficient of OA AAODs from both B2012 and C2012 was 0.70. The differences between OA AAOD from B2012 and that from C2012 were positive (negative) in the area with high (low) AAE values. That is, OA AAOD values from the method of B2012 are more sensitive to wavelength dependence of AAOD than those from C2012.

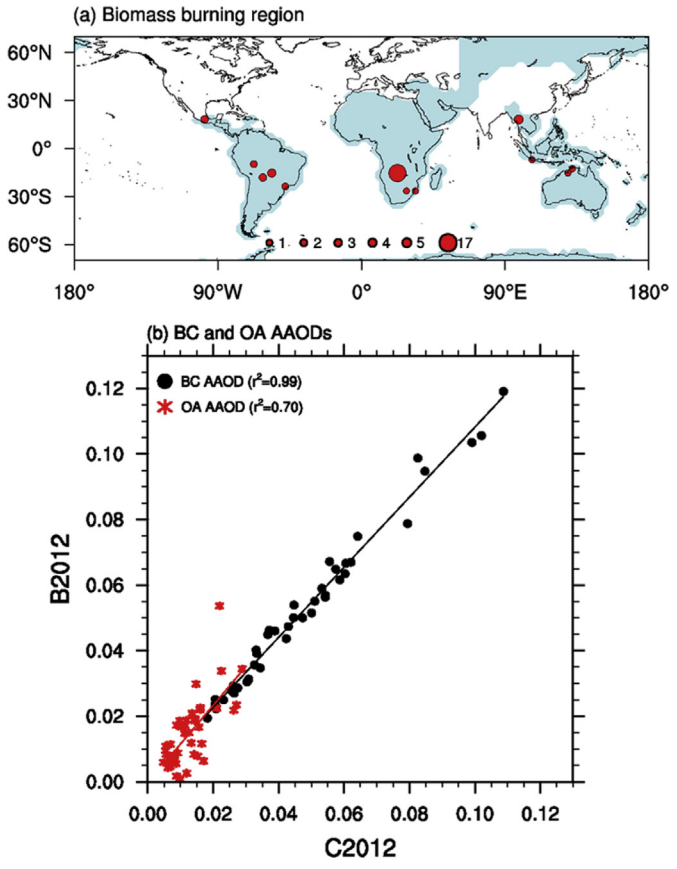

Fig. 3. (a) Aerosol Robotic Network (AERONET) sites selected as biomass burning dominated sites (red dots) based on data for the period 2001–2010. Sites dominated by biomass burning were selected according to the following criteria: single scattering albedo (SSA) < 0.85, fine-mode fraction (FMF) > 0.80, and Ångström Exponent (AE) > 1.0 over non-industrial regions, where non-industrial regions (blue shading) are roughly selected excluding Asia, Europe, and North America. The number of selected sites is 41. The dot size is proportional to the number of selected months at the same site. (b) Scatter plot of black carbon (BC) absorption aerosol optical depth (AAOD) and organic aerosol (OA) AAOD for 41 biomass-burning-dominated sites retrieved from the AAOD separation methods in Chung et al. (2012; C2012) and Bahadur et al. (2012; B2012). (For interpretation of the references to colour in this figure legend, the reader is referred to the web version of this article.)

3.1.2. Sensitivity for fine-mode sea-salt and dust

As explained in Section 2.2, we adopted the fine-mode ratio of dust + sea-salt AOD from the model simulation rather than using fdust + fss AOD directly. We validated the model performance in simulating the FMFs of dust and sea-salt in comparison with observed FMFs. For the validation, we selected dust- and sea-salt-dominated sites by using annual mean values based on the following criteria: FMF <0.35, AAE <1.5, and AAOD >0.03 for the dust-dominated sites, and FMF <0.35 and SSA >0.96 for the sea-salt-dominated sites (Fig. 4(a)). We replaced missing AERONET SSA data with those obtained by the GOCART simulation. In total, eight and three sites were selected for dust and sea-salt aerosols respectively. Fig. 4(b) and (c) show the monthly variation of both simulated and observed FMFs averaged over the chosen sites for dust and sea-salt aerosols respectively. Fig. 4(b) suggests that the range of simulated FMF are comparable to observation that has FMF values with the range of 0.21–0.47. However, the models tended to have nearly constant FMFs throughout the year and failed to simulate the observed annual cycle of high (low) values in boreal winter (summer). The multi-model mean FMF was computed by averaging the AOD and fAOD from the three models individually and by dividing fAOD into the AOD. This value of FMF was closest to that of observation. However, the observed FMF over the chosen sea-salt-dominated sites was in the range of 0.25–0.36. GOCART (TM5 and ModelE2-TOMAS) tended to overestimate (underestimate) FMF.

Fig. 5 shows a quantitative comparison of simulated fdust, fss, fdust + fss, and the fine-mode ratio of dust + sea-salt AOD from biomass-burning-dominated regions. Large model-to-model differences were noted in fdust AOD, whereas those for fss were small. The fdust AOD for TM5 was five times larger than that for the GOCART model. The large difference in fdust + fss AOD is mainly attributed to the fdust AOD. The range in the fine-mode ratio of dust + sea-salt AODs was 0.53–0.71. Therefore, our approach minimizes the model deficiencies in simulating fdust and fss AOD.

3.2. Determination of OA SSA

As mentioned earlier, we derived a new empirical relationship that binds OA SSA and sulfate + nitrate AOD in Eq. (5) or Eq. (6). In this section, we describe the process of finding a solution of Eq. (6).

At first, we calculated the ratio of sulfate + nitrate AOD to fAOD with varying OA SSA from 0 to 1 over the 41 biomass-burning-dominated sites in Fig. 3(a), and then took an average of 41 sites. Therefore, the sulfate + nitrate AOD can be described as a function of OA SSA. Three uncertainty factors including AAOD separation method, fine-mode ratio of dust + sea-salt AOD, BC SSA were took into account separately. The calculated ratio of sulfate + nitrate AOD to fAOD averaged over the 41 biomass-burning-dominated sites is given in Fig. 6. The resulting curve indicates an empirically determined relationship between the sulfate + nitrate ratio to fAOD and OA SSA. Each line depicts the relationship from different sensitivity tests. According to the equation, sulfate + nitrate AOD is proportional to (1- 1/(1-OA SSA)). In other words, the enhancement of OA absorption, i.e., the decrease in OA SSA, reflects increases the relative amount of sulfate + nitrate AOD to fAOD. Thus, the curves show inverse exponential distribution of the sulfate + nitrate ratio toward decreasing OA. On the basis of observation, it was reported that the formation of light-absorbing OA is enhanced in the presence of ammonium sulfate system, which are efficient catalysts of

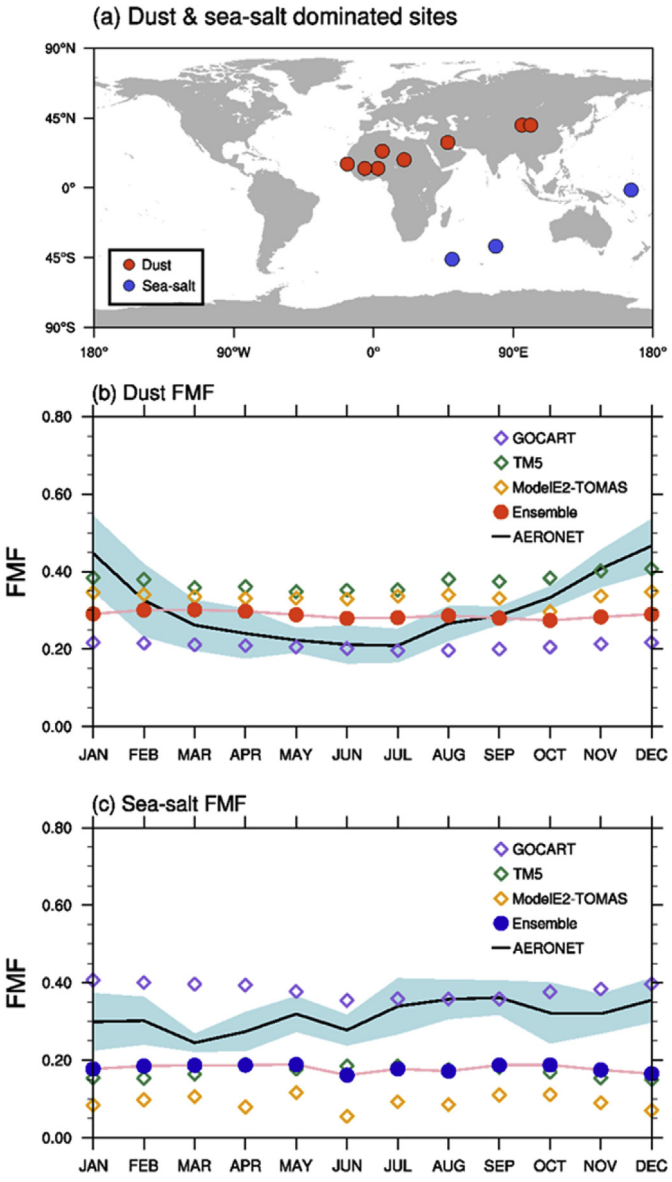

Fig. 4. (a) Chosen dust-dominated (red dots) and sea-salt-dominated (blue dots) AERONET sites. (b), (c) Monthly variation of simulated and observed dust (sea-salt) FMF averaged over the chosen dust (sea-salt) dominated sites. For observations, the total FMF is shown. The multi-model mean and ±1 standard deviation from observation are indicated by a black solid line and blue shading, respectively. The FMFs from the Goddard Chemistry Aerosol Radiation and Transport (GOCART), Tracer Model 5 (TM5), and ModelE2-*Two-Moment* Aerosol Sectional (ModelE2-TOMAS) models are indicated by purple, green, and yellow open diamonds, respectively; that of the multi-model mean is indicated by a closed circle. (For interpretation of the references to colour in this figure legend, the reader is referred to the web version of this article.)

aldol condensation reaction (Laskin et al., 2015). Song et al. (2013) also presented the results from a systematic laboratory study that light absorbing secondary OA is formed in highly acidic sulfate aerosols.

It is interesting to note that the sulfate + nitrate ratio computed from the C2012 AAOD separation method is greater than that from B2012. This is because the BC and OA AAODs from B2012 tend to be greater than those from C2012. In addition, the increased BC SSA acts to reduce the sulfate + nitrate ratio in our empirical relationship (i.e., Eq. (6)). On the contrary, the contribution of the fine-mode ratio of dust + sea-salt AOD from individual models is relatively small.

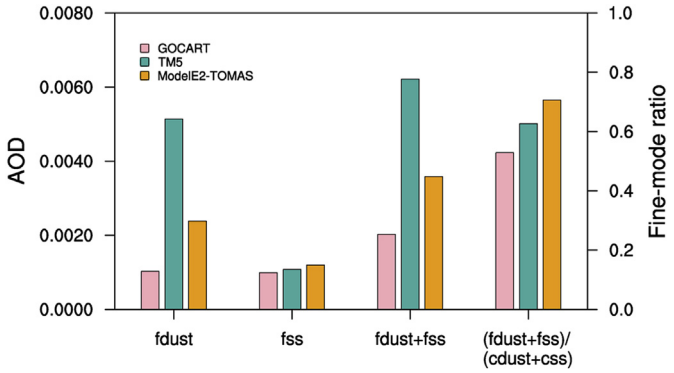

Fig. 5. Simulated fine-mode dust (fdust), fine-mode sea-salt (fss), fdust + fss aerosol optical depth (AOD) values, and the fine-mode ratio of dust + sea-salt AOD from GOCART, TM5, and ModelE2-TOMAS, respectively. The AOD and fine-mode ratio were averaged over the 41 biomass-burning-dominated sites.

Since Eq. (6) was applied to biomass-burning-dominated sites, the measured value of sulfate + nitrate AOD ratio to fAOD over biomass burning region can be used to determine OA SSA. However, few in situ measurements have been conducted over tropical biomass burning regions, and considerable uncertainties occur in the observations owing to differences in absorption measurement techniques and filter samples (Bond et al., 1999; Chow et al., 2009; Ogren et al., 2010). To the best of our knowledge, Magi (2009, 2011) synthesized previous in situ measurements of aerosol mass concentrations obtained during SAFARI-2000 and carefully calibrated the uncertainties from different filter samples. We applied Eq. (6) with its associated set of observations and simulations including fAOD, cAOD, BC AAOD, OA AAOD, and the fine-mode ratio of sea-salt + dust AOD values over the tropical biomass burning regions to the calibrated measurements in Magi (2009, 2011).

Table 4 shows the calibrated mass concentrations (M), mass absorption cross-sections (MAC), mass scattering cross-sections (MSC), and contributions to total light extinction of particular species (i) in Magi (2009, 2011, 2009, 2011) identified aerosol properties of extratropical and tropical southern Africa. During the campaign, the origin of parcels arriving from the north and west in the tropical region north of 22.5 ^{o}S are affected by fires to a greater degree than those in the extratropics. It should be noted that we used only the measurements of tropical southern Africa and recalculated the relative contribution of sulfate + nitrate AOD. The i in the table indicates aerosol species composed of particulate matter 2.5 μm or less in diameter. To calculate the mass concentration of the aerosol particles, the measured ionic species, i.e., sulfate and nitrate, are assumed for simplicity to be entirely neutralized by ammonium ($NH4^{+}$) and converted to ammonium sulfate ($(NH4)_2SO_4$) and ammonium nitrate (NH_4NO_3). The mass conversion factors for sulfate and nitrate aerosols are 1.38 and 1.29, respectively. In addition, the value of 2.1 for conversion of OC to OA (OA/OC) was used. Further details of mass conversion are given in Magi (2009, 2011).

The total aerosol scattering (SCA), absorption (ABS), and extinction (EXT) are calculated using following equations:

$$SCA = \sum_{i=1}^{4} M_i \cdot \frac{MSC_i^2}{MSC_i + MAC_i} \quad (7)$$

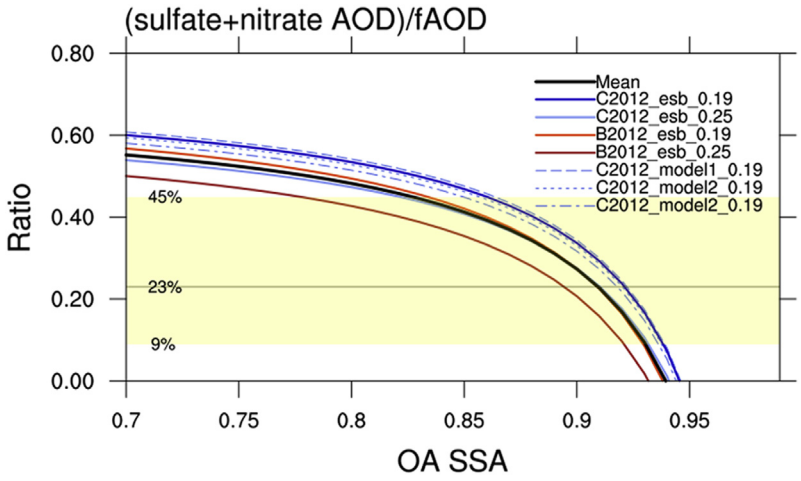

Fig. 6. Ratio of sulfate + nitrate AOD to fine-mode AOD (fAOD) profile as a function of OA SSA computed by using Eq. (6) and averaged over the 41 biomass burning sites. The AAOD separation method is from C2012 (blue lines) or from B2012 (red lines). The fine-mode ratio of dust + sea-salt AOD from individual models is marked by dotted lines. The BC SSA values are 0.19 and 0.25, as recommended by Magi (2009, 2011) and Bond and Bergstrom (2006). Black contour indicates the average of the curves. The yellow shaded area indicates the observed range of contribution of sulfate + nitrate AOD to fAOD. (For interpretation of the references to colour in this figure legend, the reader is referred to the web version of this article.)

Table 4
Mass concentration (M) ($\mu g/m^3$) and optical properties of aerosol species contributing to fine-mode aerosols ($PM_{2.5}$) measured in tropical southern Africa during the Southern African Research Initiative field campaign in August and September 2000 (SAFARI-2000). Values are adopted from the work of Magi (2009, 2011), who calibrated uncertainties from flow meters and presented credible mass concentrations for sulfate, nitrate, OA, and BC.

Species	M ($\mu g/m^3$)	MSC (m^2/g)	MAC (m^2/g)	Contribution to EXT
Sulfate	4.69 (4.28–5.24)	6.10 (4.00–8.20)	0	0.14 (0.07–0.26)
Nitrate	3.35 (1.94–3.87)	5.50 (3.40–7.60)	0	0.09 (0.03–0.19)
OA	36.00 (25.30–47.70)	3.80 (3.30–4.30)	0.70 (0.50–0.90)	0.59 (0.48–0.67)
BC	3.40 (1.80–4.50)	2.9 (2.10–3.70)	12.10 (11.30–12.90)	0.18 (0.07–0.29)

$$ABS = \sum_{i=1}^{4} M_i \cdot \frac{MAC_i^2}{MSC_i + MAC_i} \quad (8)$$

$$EXT = SCA + ABS \quad (9)$$

According to the calculated apportionment of light extinction in Table 4, the contribution of sulfate + nitrate aerosols to the total fine-mode aerosols over the tropical biomass burning region is 0.23 with a range of 0.09–0.45. The yellow box in Fig. 6 shows the observed range of contribution of sulfate + nitrate AOD to fAOD, and this provide a constraint of the reasonable OA SSA range. For the case of the AAOD separation method from C2012 and a BC SSA of 0.19, an OA SSA value of 0.92 gave a sulfate + nitrate ratio of 0.23. The lower and upper limits of OA SSA were 0.86 and 0.94. The second case, including the method of C2012 and a BC SSA of 0.25, and the third case, including the method of B2012 and a BC SSA of 0.19, showed similar curves and yielded a similar range of OA SSA with the best fit of 0.91. On the contrary, the OA SSA was 0.89 in the case the B2012 method and the BC SSA of 0.25. By taking average of four sensitivity tests as shown in thick black line in Fig. 6, we conclude that our best estimate of OA SSA is 0.91 with the range of 0.82–0.93.

Previously, many studies have tried to quantify SSA of light absorbing organic particles. For example, Chakrabarty et al. (2010) used direct observation to determine that the SSA of tar balls (Chakrabarty et al., 2006), a class of light absorbing organic carbon produced from the smoldering combustion of dry duffs, is significantly higher than 0.95 at 550 nm. Hoffer et al. (2006) measured the absorption properties of the humic-like substances (HULIS) isolated from the fine fraction of biomass burning aerosols collected in the Amazon basin and reported that the SSA of pure HULIS particles is about 0.98 at 532 nm. Contrary to weakly absorbing organic carbon measured by Chakrabarty et al. (2010) and Hoffer et al. (2006), Alexander et al. (2008) found a strongly absorbing BrC spheres, which are ubiquitous in East Asian-Pacific outflow, and they suggested that the SSA could be as low as 0.44. Although those findings have contributed to the better understanding of a subset of organic carbon, studies on quantification of OA SSA are still rare. A few studies tried to measure OA SSA from in situ filed observation and AERONET-based retrieval. Magi (2009, 2011) characterized the aerosol over southern Africa during the biomass burning season during SAFARI-2000 campaign and reported that OA SSA is 0.85 ± 0.05. Bahadur et al. (2012) provided an analytical method for rigorously partitioning measured AAOD and SSA among BC, OA and offered that OA SSA varies globally between 0.77 and 0.85.

Fig. 7 shows the SSA of OA retrieved from this study (red box), two observation-based studies (blue boxes), and that for the primary organic aerosol (POA) used in AeroCom phase II (green boxes). Some models do not include secondary organic aerosol, and therefore the SSAs of POA are only displayed. The POA SSA in most of the models except for OsloCTM2 and CAM4-Oslo varied with relative humidity or aerosol size. A brief explanation of aerosol optical properties for AeroCom phase II models is available at the AeroCom wiki site (https://wiki.met.no/aerocom/optical_properties). Detailed model description and general information can be found in Myhre et al. (2013) and Tsigaridis et al. (2014). Our OA SSA of 0.91 with the range of 0.82–0.93 is slightly higher than those from observation-based studies. The overlapped range in all

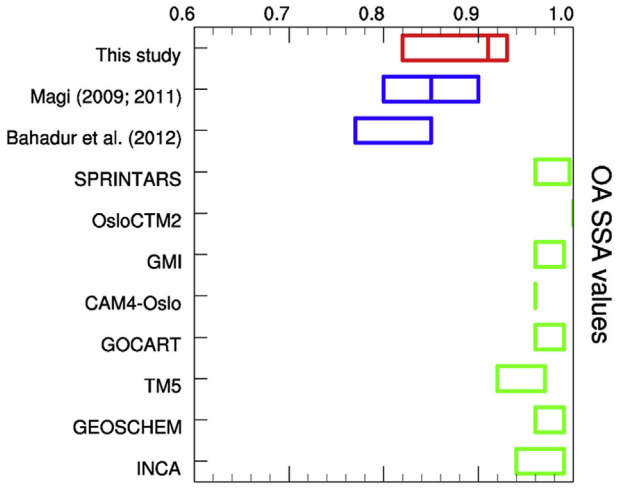

Fig. 7. OA SSA from this study (red), observation-based retrievals (blue), and primary organic aerosol SSA used in AeroCom II models (green). Solid line inside the boxes show the best estimate and the boxes indicate the range of OA SSA. (For interpretation of the references to colour in this figure legend, the reader is referred to the web version of this article.)

studies is 0.82–0.85. However, as shown in the figure, atmospheric CTMs as well as GCMs commonly use POA SSA values of 0.96–1.0. In fact, OsloCTM2, treats POA as a totally scattering species. Thus, commonly used OA SSA values of 0.96–1.0 in aerosol and climate models have been underrepresented OA light absorption. The best interpretation for the OA SSA range of 0.82–0.93 in the tropics is that the strongly-absorbing BrC (Alexander et al., 2008) or similarly absorbing BrC aerosols (Liu et al., 2013; Magi, 2009, 2011) are abundant in the tropical biomass burning areas. However, further analysis is needed to understand the mixing state of light absorbing BrC and scattering OA.

3.3. Application for global sulfate + nitrate AOD

In the previous section, we described how to obtain OA SSA from the empirical relationship between sulfate + nitrate AOD and OA SSA in Eq. (6). On the contrary, the empirical relationship can also be used to determine sulfate + nitrate AOD with a given OA SSA value. As an application of our algorithm, this section provides an observationally constrained estimate of global-scale sulfate + nitrate AOD and its implication on global aerosol simulations.

For the global-scale estimation, the global fAOD, cAOD, and AAOD are required. Previously, Lee and Chung (2013) obtained the global distribution of AOD and fAOD, and Chung et al. (2012) obtained AAOD by integrating MODIS, Multi-angle Imaging Spectroradiometer (MISR), and AERONET observations. Their integrated AOD and fAOD values are closer in accuracy to AERONET data than MODIS (or MISR) AOD and fAOD alone. We used the global distribution of AOD and fAOD from Lee and Chung (2013) and the AAOD from Chung et al. (2012) to estimate global-scale sulfate + nitrate AOD.

Fig. 8(a) shows the annual mean sulfate + nitrate AOD over the globe when OA SSA is set to our best estimate of 0.91 for the period 2001–2010. When OA SSA was set to 0.91, the highest values occurred over East Asia, and considerable amounts of sulfate + nitrate AOD were also found over eastern North America, central South America, and all of Europe. Slightly negative values were found over the oceanic area of central western Africa and the Middle East. However, when we adopted an OA SSA value of 0.97,

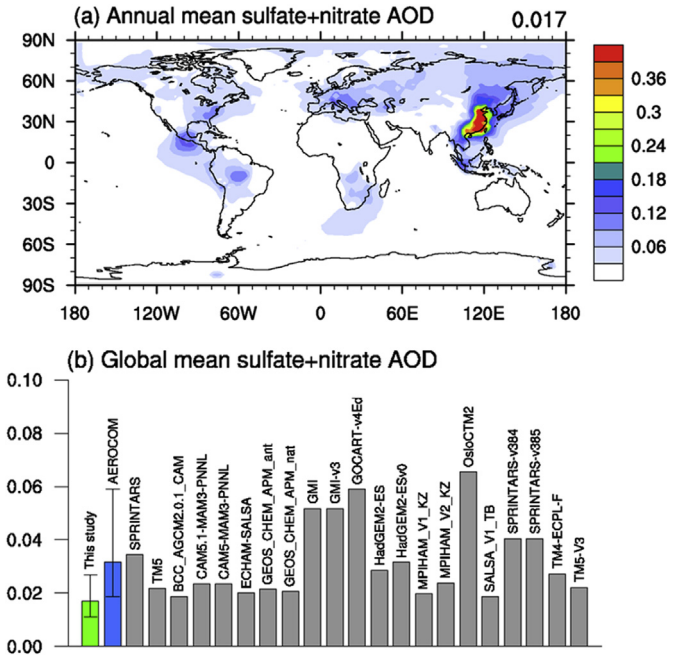

Fig. 8. (a) Global distribution of annual mean sulfate + nitrate AOD using our best estimate when OA SSA is 0.91 for the period 2001–2010. (b) Comparison of our global and annual mean sulfate + nitrate AOD with that of 21 models participated in AeroCom phase II. The green box (leftmost) is our best estimate, the blue box is from the model average, and the others are for individual models. If the nitrate aerosol of the model is missing, the nitrate aerosol averaged from two models is used. The error bar for our estimate denotes the uncertainties from the range of BC SSA (0.19–0.25) and OA SSA (0.82–0.93) whereas that of AeroCom denotes the upper 90 and lower 10 percentiles of 21 models. (For interpretation of the references to colour in this figure legend, the reader is referred to the web version of this article.)

negative sulfate + nitrate AOD was found over nearly all of Africa and the middle and southern Asia (figure not shown). This unrealistic representation of sulfate + nitrate AOD occurred because these negative areas contain a very small amount of sulfate + nitrate amount but a considerable amount of OAs. We suspect that this negative bias arose from the failure of the models to simulate the annual cycle of dust FMF. Because the AOD over the Sahara desert area has an annual cycle opposite that of the FMF, the failure of simulating the dust FMF leads to an overestimation of the dust fAOD.

We also compared our global estimate of sulfate + nitrate AOD with that of 21 global aerosol models participated in AeroCom phase II. Because most models do not include nitrate AOD, we added that component to these models, as discussed in Section 2.1.3. Fig. 8(b) shows the global and annual mean sulfate + nitrate AOD obtained from our empirical approach and individual models. Considering the ranges of OA SSA and BC SSA of 0.82–0.93 and 0.19–0.25 respectively, our observationally constrained estimates of the global average sulfate + nitrate AOD gave a range of 0.011–0.027 with a mean value of 0.017. On the other hand, the 21 models gave a global average sulfate + nitrate AOD of 0.019–0.059 in the upper 90 and lower 10 percentiles. The observational estimate of the global average sulfate + nitrate AOD 0.017 was close to the lower end of the simulated range of 0.019–0.059, which indicates that many aerosol models overestimate the sulfate + nitrate amount.

Previously, Kinne et al. (2006) have compared annual global AOD values from remote sensing including AERONET and satellite to those obtained from 20 different AeroCom model simulations. They reported that models overestimate the AOD values for Europe

during the summer months, Northeast Asia in off-dust seasons, and US during the winter months. The overestimated AOD values are confined to the industrial regions where sulfate and nitrate aerosols are the main constituents of the atmospheric particulate matter. Therefore, the result supports our argument that AeroCom models overestimate sulfate + nitrate AOD. Our final results, i.e., underrepresented OA light absorption and overrepresented sulfate + nitrate scattering in global aerosol models, suggest that direct aerosol forcing is less negative (or more positive) than that currently believed.

4. Conclusion

We developed an empirical method for determining OA SSA over the tropical biomass burning regions. A simplified process flow chart for deriving OA SSA is described in Fig. 2. The basic concept of the method is that atmospheric fine particles are composed of sulfate + nitrate, BC, OA, fdust, and fss. By using fAOD and AAOD data from the monthly ground-based AERONET observation, we formulated an equation for sulfate + nitrate AOD as a function of OA SSA with the optically separated BC and OA AAODs from total AAOD and the measured BC SSA. We derived two sets of observationally constrained AAOD separation methods from C2012 and B2012. With regard to BC SSA, we used two measured values of 0.25 from Bond and Bergstrom (2006) and 0.19 from Magi (2009, 2011). For the fdust and fss AODs, a semi-observational approach was proposed that obtains their AOD by multiplying the fine-mode ratio of dust + sea-salt AOD from the multi-model mean by the observed cAOD. Although the multi-model mean fine-mode ratio of dust + sea-salt AOD was used, their contribution to sulfate + nitrate AOD was relatively small. Therefore, the final equation, i.e., Eq. (5) or its applied version in Eq. (6), is predominantly an observationally constrained approach in which the equation to determine the sulfate + nitrate AOD has a sole parameter (i.e., OA SSA). Our empirical method for determining OA SSA contains three independent uncertainty factors in (1) separating BC and OA AAODs from the total AAOD, (2) using model simulations for fdust and fss AODs, and (3) adopting the measured BC SSA. A quantitative comparison of these factors in determining sulfate + nitrate AOD and OA SSA was presented in detail.

We applied the equation to the 41 chosen biomass burning sites. The final OA SSA was determined by the measured sulfate + nitrate AOD in Magi (2009, 2011), or more precisely, the ratio of sulfate + nitrate AOD to fAOD, which synthesized previous in situ measurements of aerosol mass concentrations obtained during SAFARI-2000 and carefully calibrated uncertainties from different filter samples. Our best estimate of OA SSA in the tropical biomass burning region is 0.91 with the range of 0.82–0.93. This result implies that commonly used OA SSA values of 0.96–1.0 in aerosol and climate models (Fig. 7) significantly underrepresent OA light absorption. The interpretation for the OA SSA value of 0.82–0.93 in the regions dominated by biomass burning is that strongly absorbing BrC (Alexander et al., 2008) or similarly absorbing BrC aerosols (Liu et al., 2013; Magi, 2009, 2011) are abundant in tropical areas.

This work marks the first time that observational estimates of the global-scale sulfate + nitrate AOD are produced. The global estimation was made by using the global fAOD from Lee and Chung (2013) and the AAOD from Chung et al. (2012), who integrated satellite and ground-based AERONET observations. For comparison with empirically determined global mean sulfate + nitrate AOD, we compiled sulfate + nitrate AOD simulations from 21 global aerosol models in AeroCom phase II. These models gave global average sulfate + nitrate AOD values of 0.019–0.059. The observationally estimated sulfate + nitrate AOD of 0.017 with a range of 0.011–0.027 is near the lower end of the simulated range of 0.019–0.059, which strongly suggests that many aerosol models overestimate the sulfate + nitrate amount.

This study has some limitations which have to be pointed out. In determining OA SSA, We used the value of sulfate + nitrate contribution to fine aerosols relying on single field campaign by Magi (2009, 2011). For the evaluation of OA SSA in other biomass burning regions, more measurements are highly required. In addition, the derived OA SSA is suitable for monthly mean state. In other words, the understanding of their aging process in the atmosphere and its influence on the optical characteristics are still lacking. In spite of the above mentioned limitations, we would like to conclude that the approach in this study is a unique and creative method to quantify OA light absorption constrained mostly by ground-based AERONET observation.

Our results provide strong evidence that aerosol models have underestimated the OA light absorption substantially and tend to overestimate the amount of sulfate + nitrate aerosols. This implies that the aerosol light absorption underrepresented. Recently, Myhre et al. (2013) analyzed numerous aerosol simulation models in AeroCom, which is an intercomparison exercise of a large set of global aerosol models that includes extensive evaluation against measurements. The range of direct radiative forcing reported in AeroCom was an important basis for the recent IPCC conclusion on direct aerosol radiative forcing (IPCC, 2013). The IPCC fifth assessment report provided that global and annual mean radiative forcing due to interaction between biomass burning aerosol and radiation is estimated to be 0.0 W m^{-2} with a range of −0.20 to +0.20 W m^{-2} (IPCC, 2013). The present study suggests that actual direct aerosol forcing is less negative (or more positive) than that currently believed. We believe the observation-based retrieval of OA optical properties in this study contributes to constraining the current radiative forcing by OA light absorption.

Acknowledgements

The authors would like to thank Dr. C. E. Chung for his helpful comments on the early manuscript. This work was supported by National Research Foundation (NRF) Grants for Fostering Core Leaders of the Future Basic Science Program (NRF-2013H1A8A1004201) and GRL grant (MEST 2011-0021927) by the Korean Government.

References

Abel, S.J., Highwood, E.J., Haywood, J.M., Stringer, M.A., 2005. The direct radiative effect of biomass burning aerosols over southern Africa. Atmos. Chem. Phys. 5, 1999–2018. http://dx.doi.org/10.5194/acp-5-1999-2005.

Adams, P.J., Seinfeld, J.H., 2002. Predicting global aerosol size distributions in general circulation models. J. Geophys. Res. 107, 4–23. http://dx.doi.org/10.1029/2001JD001010. AAC 4-1-AAC.

Alexander, D.T., Crozier, P.A., Anderson, J.R., 2008. Brown carbon spheres in East Asian outflow and their optical properties. Science 321, 833–836. http://dx.doi.org/10.1126/science.1155296.

Andreae, M.O., Gelencsér, A., 2006. Black carbon or brown carbon? The nature of light-absorbing carbonaceous aerosols. Atmos. Chem. Phys. 6, 3131–3148. http://dx.doi.org/10.5194/acp-6-3131-2006.

Bahadur, R., Praveen, P.S., Xu, Y., Ramanathan, V., 2012. Solar absorption by elemental and brown carbon determined from spectral observations. Proc. Natl. Acad. Sci. U. S. A. 109, 17366–17371. http://dx.doi.org/10.1073/pnas.1205910109.

Bond, T.C., 2001. Spectral dependence of visible light absorption by carbonaceous particles emitted from coal combustion. Geophys. Res. Lett. 28, 4075–4078. http://dx.doi.org/10.1029/2001GL013652.

Bond, T.C., Anderson, T.L., Campbell, D., 1999. Calibration and intercomparison of filter-based measurements of visible light absorption by aerosols. Aerosol Sci. Technol. 30, 582–600. http://dx.doi.org/10.1080/027868299304435.

Bond, T.C., Bergstrom, R.W., 2006. Light absorption by carbonaceous particles: an investigative review. Aerosol Sci. Technol. 40, 27–67. http://dx.doi.org/10.1080/02786820500421521.

Boucher, O., Randall, D., Artaxo, P., Bretherton, C., Feingold, G., Forster, P., Kerminen, V.-M., Kondo, Y., Liao, H., Lohmann, U., Rasch, P., Satheesh, S.K.,

Sherwood, S., Stevens, B., Zhang, X.Y., 2013. Clouds and aerosols. In: Stocker, T.F., Qin, D., Plattner, G.-K., Tignor, M., Allen, S.K., Boschung, J., Nauels, A., Xia, Y., Bex, V., Midgley, P.M. (Eds.), Climate Change 2013: the Physical Science Basis. Contribution of Working Group I to the Fifth Assessment Report of the Intergovernmental Panel on Climate Change. Cambridge University Press, Cambridge, United Kingdom and New York, NY, USA, pp. 571–658.

Chakrabarty, R.K., Moosmüller, H., Chen, L.W.A., Lewis, K., Arnott, W.P., Mazzoleni, C., Dubey, M.K., Wold, C.E., Hao, W.M., Kreidenweis, S.M., 2010. Brown carbon in tar balls from smoldering biomass combustion. Atmos. Chem. Phys. 10, 6363–6370. http://dx.doi.org/10.5194/acp-10-6363-2010.

Chakrabarty, R.K., Moosmüller, H., Garro, M.A., Arnott, W.P., Walker, J., Susott, R.A., Babbitt, R.E., Wold, C.E., Lincoln, E.N., Hao, W.M., 2006. Emissions from the laboratory combustion of wildland fuels: particle morphology and size. J. Geophys. Res. 111 http://dx.doi.org/10.1029/2005JD006659.

Chen, Y., Bond, T.C., 2010. Light absorption by organic carbon from wood combustion. Atmos. Chem. Phys. 10, 1773–1787. http://dx.doi.org/10.5194/acp-10-1773-2010.

Chin, M., Ginoux, P., Kinne, S., Torres, O., Holben, B.N., Duncan, B.N., Martin, R.V., Logan, J.A., Higurashi, A., Nakajima, T., 2002. Tropospheric aerosol optical thickness from the GOCART model and comparisons with satellite and sun photometer measurements. J. Atmos. Sci. 59, 461–483. http://dx.doi.org/10.1175/1520-0469(2002)059<0461:TAOTFT>2.0.CO;2.

Chow, J.C., Watson, J.G., Doraiswamy, P., Chen, L.-W.A., Sodeman, D.A., Lowenthal, D.H., Park, K., Arnott, W.P., Motallebi, N., 2009. Aerosol light absorption, black carbon, and elemental carbon at the Fresno Supersite, California. Atmos. Res. 93, 874–887. http://dx.doi.org/10.1016/j.atmosres.2009.04.010.

Chung, C.E., Ramanathan, V., Decremer, D., 2012. Observationally constrained estimates of carbonaceous aerosol radiative forcing. Proc. Natl. Acad. Sci. U. S. A. 109, 11624–11629. http://dx.doi.org/10.1073/pnas.1203707109.

Cross, E.S., Onasch, T.B., Ahern, A., Wrobel, W., Slowik, J.G., Olfert, J., Lack, D.A., Massoli, P., Cappa, C.D., Schwarz, J.P., Spackman, J.R., Fahey, D.W., Sedlacek, A., Trimborn, A., Jayne, J.T., Freedman, A., Williams, L.R., Ng, N.L., Mazzoleni, C., Dubey, M., Brem, B., Kok, G., Subramanian, R., Freitag, S., Clarke, A., Thornhill, D., Marr, L.C., Kolb, C.E., Worsnop, D.R., Davidovits, P., 2010. Soot particle studies—instrument inter-comparison—project overview. Aerosol Sci. Technol. 44, 592–611. http://dx.doi.org/10.1080/02786826.2010.482113.

Dubovik, O., Holben, B., Eck, T.F., Smirnov, A., Kaufman, Y.J., King, M.D., Tanré, D., Slutsker, I., 2002. Variability of absorption and optical properties of key aerosol types observed in worldwide locations. J. Atmos. Sci. 59, 590–608. http://dx.doi.org/10.1175/1520-0469(2002)059<0590:VOAAOP>2.0.CO;2.

Eck, T.F., Holben, B.N., Reid, J.S., Dubovik, O., Smirnov, A., O'Neill, N.T., Slutsker, I., Kinne, S., 1999. Wavelength dependence of the optical depth of biomass burning, urban, and desert dust aerosols. J. Geophys. Res. 104, 31333–31349. http://dx.doi.org/10.1029/1999JD900923.

Feng, Y., Ramanathan, V., Kotamarthi, V.R., 2013. Brown carbon: a significant atmospheric absorber of solar radiation? Atmos. Chem. Phys. 13, 8607–8621. http://dx.doi.org/10.5194/acp-13-8607-2013.

Forrister, H., Liu, J., Scheuer, E., Dibb, J., Ziemba, L., Thornhill, K.L., Anderson, B., Diskin, G., Perring, A.E., Schwarz, J.P., Campuzano-Jost, P., Day, D.A., Palm, B.B., Jimenez, J.L., Nenes, A., Weber, R.J., 2015. Evolution of brown carbon in wildfire plumes. Geophys. Res. Lett. 42, 4623–4630. http://dx.doi.org/10.1002/2015gl063897.

Giglio, L., Randerson, J.T., van der Werf, G.R., 2013. Analysis of daily, monthly, and annual burned area using the fourth-generation global fire emissions database (GFED4). J. Geophys. Res. 118, 317–328. http://dx.doi.org/10.1002/jgrg.20042.

Giles, D.M., Holben, B.N., Eck, T.F., Sinyuk, A., Smirnov, A., Slutsker, I., Dickerson, R.R., Thompson, A.M., Schafer, J.S., 2012. An analysis of AERONET aerosol absorption properties and classifications representative of aerosol source regions. J. Geophys. Res. 117 http://dx.doi.org/10.1029/2012jd018127.

Hess, M., Koepke, P., Schult, I., 1998. Optical properties of aerosols and clouds: the software package OPAC. Bull. Amer. Meteorol. Soc. 79, 831–844. http://dx.doi.org/10.1175/1520-0477(1998)079<0831:OPOAAC>2.0.CO;2.

Hoffer, A., Gelencsér, A., Guyon, P., Kiss, G., Schmid, O., Frank, G.P., Artaxo, P., Andreae, M.O., 2006. Optical properties of humic-like substances (HULIS) in biomass-burning aerosols. Atmos. Chem. Phys. 6, 3563–3570. http://dx.doi.org/10.5194/acp-6-3563-2006.

Holben, B.N., Eck, T.F., Slutsker, I., Tanré, D., Buis, J.P., Setzer, A., Vermote, E., Reagan, J.A., Kaufman, Y.J., Nakajima, T., Lavenu, F., Jankowiak, I., Smirnov, A., 1998. AERONET- a federated instrument network and data archive for aerosol characterization. Remote Sens. Environ. 66, 1–16. http://dx.doi.org/10.1016/S0034-4257(98)00031-5.

Holben, B.N., Tanré, D., Smirnov, A., Eck, T.F., Slutsker, I., Abuhassan, N., Newcomb, W.W., Schafer, J.S., Chatenet, B., Lavenu, F., Kaufman, Y.J., Castle, J.V., Setzer, A., Markham, B., Clark, D., Frouin, R., Halthore, R., Karneli, A., O'Neill, N.T., Pietras, C., Pinker, R.T., Voss, K., Zibordi, G., 2001. An emerging ground-based aerosol climatology: aerosol optical depth from AERONET. J. Geophys. Res. 106, 12067–12097. http://dx.doi.org/10.1029/2001jd900014.

Huijnen, V., Williams, J., van Weele, M., van Noije, T., Krol, M., Dentener, F., Segers, A., Houweling, S., Peters, W., de Laat, J., Boersma, F., Bergamaschi, P., van Velthoven, P., Le Sager, P., Eskes, H., Alkemade, F., Scheele, R., Nédélec, P., Pätz, H.W., 2010. The global chemistry transport model TM5: description and evaluation of the tropospheric chemistry version 3.0. Geosci. Model Dev. 3, 445–473. http://dx.doi.org/10.5194/gmd-3-445-2010.

IPCC, 2013. In: Stocker, T.F., Qin, D., Plattner, G.-K., Tignor, M., Allen, S.K., Boschung, J., Nauels, A., Xia, Y., Bex, V., Midgley, P.M. (Eds.), Climate Change 2013: the Physical Science Basis: Working Group I Contribution to the Fifth Assessment Report of the Intergovernmental Panel on Climate Change. Cambridge University Press.

Kanakidou, M., Seinfeld, J.H., Pandis, S.N., Barnes, I., Dentener, F.J., Facchini, M.C., Van Dingenen, R., Ervens, B., Nenes, A., Nielsen, C.J., Swietlicki, E., Putaud, J.P., Balkanski, Y., Fuzzi, S., Horth, J., Moortgat, G.K., Winterhalter, R., Myhre, C.E.L., Tsigaridis, K., Vignati, E., Stephanou, E.G., Wilson, J., 2005. Organic aerosol and global climate modelling: a review. Atmos. Chem. Phys. 5, 1053–1123. http://dx.doi.org/10.5194/acp-5-1053-2005.

Kinne, S., Schulz, M., Textor, C., Guibert, S., Balkanski, Y., Bauer, S.E., Berntsen, T., Berglen, T.F., Boucher, O., Chin, M., Collins, W., Dentener, F., Diehl, T., Easter, R., Feichter, J., Fillmore, D., Ghan, S., Ginoux, P., Gong, S., Grini, A., Hendricks, J., Herzog, M., Horowitz, L., Isaksen, I., Iversen, T., Kirkevåg, A., Kloster, S., Koch, D., Kristjansson, J.E., Krol, M., Lauer, A., Lamarque, J.F., Lesins, G., Liu, X., Lohmann, U., Montanaro, V., Myhre, G., Penner, J., Pitari, G., Reddy, S., Seland, O., Stier, P., Takemura, T., Tie, X., 2006. An AeroCom initial assessment – optical properties in aerosol component modules of global models. Atmos. Chem. Phys. 6, 1815–1834. http://dx.doi.org/10.5194/acp-6-1815-2006.

Kirchstetter, T.W., Novakov, T., Hobbs, P.V., 2004. Evidence that the spectral dependence of light absorption by aerosols is affected by organic carbon. J. Geophys. Res. 109, 21201–21212. http://dx.doi.org/10.1029/2004JD004999. D21208.

Lack, D.A., Bahreni, R., Langridge, J.M., Gilman, J.B., Middlebrook, A.M., 2013. Brown carbon absorption linked to organic mass tracers in biomass burning particles. Atmos. Chem. Phys. 13, 2415–2422. http://dx.doi.org/10.5194/acp-13-2415-2013.

Lack, D.A., Langridge, J.M., Bahreini, R., Cappa, C.D., Middlebrook, A.M., Schwarz, J.P., 2012. Brown carbon and internal mixing in biomass burning particles. Proc. Natl. Acad. Sci. U. S. A. 109, 14802–14807. http://dx.doi.org/10.1073/pnas.1206575109.

Laskin, A., Laskin, J., Nizkorodov, S.A., 2015. Chemistry of atmospheric brown carbon. Chem. Rev. 115, 4335–4382. http://dx.doi.org/10.1021/cr5006167.

Laskin, J., Laskin, A., Nizkorodov, S.A., Roach, P., Eckert, P., Gilles, M.K., Wang, B., Lee, H.J., Hu, Q., 2014. Molecular selectivity of brown carbon chromophores. Environ. Sci. Technol. 48, 12047–12055. http://dx.doi.org/10.1021/es503432r.

Lee, K., Chung, C.E., 2013. Observationally-constrained estimates of global fine-mode AOD. Atmos. Chem. Phys. 13, 2907–2921. http://dx.doi.org/10.5194/acp-13-2907-2013.

Lee, Y.H., Adams, P.J., Shindell, D.T., 2015. Evaluation of the global aerosol microphysical ModelE2-TOMAS model against satellite and ground-based observations. Geosci. Model Dev. 8, 631–667. http://dx.doi.org/10.5194/gmd-8-631-2015.

Liu, J., Bergin, M., Guo, H., King, L., Kotra, N., Edgerton, E., Weber, R.J., 2013. Size-resolved measurements of brown carbon in water and methanol extracts and estimates of their contribution to ambient fine-particle light absorption. Atmos. Chem. Phys. 13, 12389–12404. http://dx.doi.org/10.5194/acp-13-12389-2013.

Magi, B.I., 2009. Chemical apportionment of southern African aerosol mass and optical depth. Atmos. Chem. Phys. 9, 7643–7655. http://dx.doi.org/10.5194/acp-9-7643-2009.

Magi, B.I., 2011. Corrigendum to "Chemical apportionment of southern African aerosol mass and optical depth" published in Atmos. Chem. Phys., 9, 7643–7655, 2009. Atmos. Chem. Phys. 11, 4777–4778. http://dx.doi.org/10.5194/acp-11-4777-2011.

Magi, B.I., Fu, Q., Redemann, J., Schmid, B., 2008. Using aircraft measurements to estimate the magnitude and uncertainty of the shortwave direct radiative forcing of southern African biomass burning aerosol. J. Geophys. Res. 113, D05213. http://dx.doi.org/10.1029/2007JD009258.

Myhre, G., Samset, B.H., Schulz, M., Balkanski, Y., Bauer, S., Berntsen, T.K., Bian, H., Bellouin, N., Chin, M., Diehl, T., Easter, R.C., Feichter, J., Ghan, S.J., Hauglustaine, D., Iversen, T., Kinne, S., Kirkevåg, A., Lamarque, J.F., Lin, G., Liu, X., Lund, M.T., Luo, G., Ma, X., van Noije, T., Penner, J.E., Rasch, P.J., Ruiz, A., Seland, Ø., Skeie, R.B., Stier, P., Takemura, T., Tsigaridis, K., Wang, P., Wang, Z., Xu, L., Yu, H., Yu, F., Yoon, J.H., Zhang, K., Zhang, H., Zhou, C., 2013. Radiative forcing of the direct aerosol effect from AeroCom Phase II simulations. Atmos. Chem. Phys. 13, 1853–1877. http://dx.doi.org/10.5194/acp-13-1853-2013.

Nakayama, T., Sato, K., Matsumi, Y., Imamura, T., Yamazaki, A., Uchiyama, A., 2013. Wavelength and NOx dependent complex refractive index of SOAs generated from the photooxidation of toluene. Atmos. Chem. Phys. 13, 531–545. http://dx.doi.org/10.5194/acp-13-531-2013.

Ogren, J.A., 2010. Comment on "calibration and intercomparison of filter-based measurements of visible light absorption by aerosols". Aerosol Sci. Technol. 44, 589–591. http://dx.doi.org/10.1080/02786826.2010.482111.

O'Neill, N.T., 2003. Spectral discrimination of coarse and fine mode optical depth. J. Geophys. Res. 108 http://dx.doi.org/10.1029/2002jd002975.

O'Neill, N.T., Dubovik, O., Eck, T.F., 2001a. Modified Ångström exponent for the characterization of submicrometer aerosols. Appl. Opt. 40, 2368–2375. http://dx.doi.org/10.1364/AO.40.002368.

O'Neill, N.T., Eck, T.F., Holben, B.N., Smirnov, A., Dubovik, O., Royer, A., 2001b. Bimodal size distribution influences on the variation of Angstrom derivatives in spectral and optical depth space. J. Geophys. Res. 106, 9787–9806. http://dx.doi.org/10.1029/2000jd900245.

Park, R.S., Lee, S., Shin, S.K., Song, C.H., 2014. Contribution of ammonium nitrate to aerosol optical depth and direct radiative forcing by aerosols over East Asia. Atmos. Chem. Phys. 14, 2185–2201. http://dx.doi.org/10.5194/acp-14-2185-2014.

Reid, J.S., Koppmann, R., Eck, T.F., Eleuterio, D.P., 2005. A review of biomass burning emissions part II: intensive physical properties of biomass burning particles. Atmos. Chem. Phys. 5, 799–825. http://dx.doi.org/10.5194/acp-5-799-2005.

Russell, P.B., Bergstrom, R.W., Shinozuka, Y., Clarke, A.D., DeCarlo, P.F., Jimenez, J.L., Livingston, J.M., Redemann, J., Dubovik, O., Strawa, A., 2010. Absorption Angstrom Exponent in AERONET and related data as an indicator of aerosol composition. Atmos. Chem. Phys. 10, 1155–1169. http://dx.doi.org/10.5194/acp-10-1155-2010.

Schulz, M., Chin, M., Kinne, S., 2009. The aerosol model comparison project, AeroCom, phase II: clearing up diversity. IGAC Newsl. 41, 2–11.

Schulz, M., Textor, C., Kinne, S., Balkanski, Y., Bauer, S., Berntsen, T., Berglen, T., Boucher, O., Dentener, F., Guibert, S., Isaksen, I.S.A., Iversen, T., Koch, D., Kirkevåg, A., Liu, X., Montanaro, V., Myhre, G., Penner, J.E., Pitari, G., Reddy, S., Seland, Ø., Stier, P., Takemura, T., 2006. Radiative forcing by aerosols as derived from the AeroCom present-day and pre-industrial simulations. Atmos. Chem. Phys. 6, 5225–5246. http://dx.doi.org/10.5194/acp-6-5225-2006.

Song, C., Gyawali, M., Zaveri, R.A., Shilling, J.E., Arnott, W.P., 2013. Light absorption by secondary organic aerosol from α-pinene: effects of oxidants, seed aerosol acidity, and relative humidity. J. Geophys. Res. 118, 11,741–711,749. http://dx.doi.org/10.1002/jgrd.50767.

Swap, R.J., Annegarn, H.J., Suttles, J.T., King, M.D., Platnick, S., Privette, J.L., Scholes, R.J., 2003. Africa burning: a thematic analysis of the southern african regional science initiative (SAFARI 2000). J. Geophys. Res. 108 http://dx.doi.org/10.1029/2003JD003747.

Takemura, T., Nakajima, T., Dubovik, O., Holben, B.N., Kinne, S., 2002. Single-scattering albedo and radiative forcing of various aerosol species with a global three-dimensional model. J. Clim. 15, 333–352. http://dx.doi.org/10.1175/1520-0442(2002)015<0333:SSAARF>2.0.CO;2.

Tsigaridis, K., Daskalakis, N., Kanakidou, M., Adams, P.J., Artaxo, P., Bahadur, R., Balkanski, Y., Bauer, S.E., Bellouin, N., Benedetti, A., Bergman, T., Berntsen, T.K., Beukes, J.P., Bian, H., Carslaw, K.S., Chin, M., Curci, G., Diehl, T., Easter, R.C., Ghan, S.J., Gong, S.L., Hodzic, A., Hoyle, C.R., Iversen, T., Jathar, S., Jimenez, J.L., Kaiser, J.W., Kirkevåg, A., Koch, D., Kokkola, H., Lee, Y.H., Lin, G., Liu, X., Luo, G., Ma, X., Mann, G.W., Mihalopoulos, N., Morcrette, J.J., Müller, J.F., Myhre, G., Myriokefalitakis, S., Ng, N.L., O'Donnell, D., Penner, J.E., Pozzoli, L., Pringle, K.J., Russell, L.M., Schulz, M., Sciare, J., Seland, Ø., Shindell, D.T., Sillman, S., Skeie, R.B., Spracklen, D., Stavrakou, T., Steenrod, S.D., Takemura, T., Tiitta, P., Tilmes, S., Tost, H., van Noije, T., van Zyl, P.G., von Salzen, K., Yu, F., Wang, Z., Wang, Z., Zaveri, R.A., Zhang, H., Zhang, K., Zhang, Q., Zhang, X., 2014. The AeroCom evaluation and intercomparison of organic aerosol in global models. Atmos. Chem. Phys. 14, 10845–10895. http://dx.doi.org/10.5194/acp-14-10845-2014.

Wang, Y., Zhang, Q.Q., He, K., Zhang, Q., Chai, L., 2013. Sulfate-nitrate-ammonium aerosols over China: response to 2000–2015 emission changes of sulfur dioxide, nitrogen oxides, and ammonia. Atmos. Chem. Phys. 13, 2635–2652. http://dx.doi.org/10.5194/acp-13-2635-2013.

Yamamoto, G., Tanaka, M., 1972. Increase of global albedo due to air pollution. J. Atmos. Sci. 29, 1405–1412. http://dx.doi.org/10.1175/1520-0469(1972)029<1405:IOGADT>2.0.CO;2.

Yang, M., Howell, S.G., Zhuang, J., Huebert, B.J., 2009. Attribution of aerosol light absorption to black carbon, brown carbon, and dust in China – interpretations of atmospheric measurements during EAST-AIRE. Atmos. Chem. Phys. 9, 2035–2050. http://dx.doi.org/10.5194/acp-9-2035-2009.

Yu, L., Smith, J., Laskin, A., Anastasio, C., Laskin, J., Zhang, Q., 2014. Chemical characterization of SOA formed from aqueous-phase reactions of phenols with the triplet excited state of carbonyl and hydroxyl radical. Atmos. Chem. Phys. 14, 13801–13816. http://dx.doi.org/10.5194/acp-14-13801-2014.

Zhang, X., Lin, Y.-H., Surratt, J.D., Zotter, P., Prévôt, A.S.H., Weber, R.J., 2011. Light-absorbing soluble organic aerosol in Los Angeles and Atlanta: a contrast in secondary organic aerosol. Geophys. Res. Lett. 38 http://dx.doi.org/10.1029/2011gl049385.